

Inconsistent Surface Registration via Optimization of Mapping Distortions

Di Qiu and Lok Ming Lui

Received: date / Accepted: date

Abstract We address the problem of registering two surfaces, of which a natural bijection between them does not exist. More precisely, only a partial subset of the source domain is assumed to be in correspondence with a subset of the target domain. We call such a problem an *inconsistent surface registration* problem. This problem is challenging as the corresponding regions on each surfaces and a meaningful bijection between them have to be simultaneously determined. In this paper, we propose a variational model to solve the inconsistent surface registration problem by minimizing mapping distortions. Mapping distortions are described by the Beltrami coefficient as well as the differential of the mapping. Registration is then guided by feature landmarks and/or intensities, such as curvatures, defined on each surfaces. The key idea of the approach is to control angle and scale distortions via quasiconformal theory as well as minimizing landmark and/or intensity mismatch. A splitting method is proposed to iteratively search for the optimal corresponding regions as well as the optimal bijection between them. Bijectivity of the mapping is easily enforced by a thresholding of the Beltrami coefficient. We test the proposed method on both synthetic and real examples. Experimental results demonstrate the efficacy of our proposed model.

Keywords Inconsistent surface registration; mapping distortions; Beltrami coefficient; mapping optimization problem; quasiconformal theories

1 Introduction

Surface registration aims to find meaningful pointwise correspondence between two geometric objects embedded in \mathbb{R}^3 . It has important applications in various fields, such as in computer graphics, computer vision and medical imaging. For instances, the surface registration problem in computer vision and graphics aims to find point-wise correspondence in order to perform shape analysis, relational learning, to transfer motions, textures between shapes; in medical imaging, it is necessary to find bijective dense correspondence between the target and the template anatomical surfaces so that the data defined on the surfaces can be compared meaningfully in medical analysis. Very often, a desirable registration map should be much more complex than a global rigid or affine motion.

Due to its importance, various registration models have been proposed. Existing approaches usually assume a global bijection between the two surfaces to be registered if the surfaces are closed without boundary. For the registration between open domains, prescribed boundary condition is usually imposed. In a practical situation, a natural bijection between two shapes may not exist. Usually, only a partial region of the source surface is in correspondence with a subset of the target surface. This problem arises in many real situations, such as surface stitching, surface matching of anatomical structures and so on. We refer this kind of registration problem as the *inconsistent surface registration* problem. To solve the problem, the corresponding regions on each surfaces as well as a meaningful bijection between them have to be simultaneously found. It poses a great challenge to the inconsistent surface registration problem. Mathematically, this problem can be formulated as follows. Given two

Qiu Di and Lok Ming Lui

Department of Mathematics, The Chinese University of Hong Kong, Shatin, New Territories, Hong Kong

surfaces S_1 and S_2 to be registered, we look for optimal subsets $\Omega_1 \subset S_1$ and $\Omega_2 \subset S_2$, as well as an optimal bijection $f : \Omega_1 \rightarrow \Omega_2$ that satisfies some prescribed mapping constraints. The mapping constraints are often given by feature landmarks and intensities, such as surface curvatures, defined on each surfaces. The inconsistent surface registration problem can then be described as the following optimization problem:

$$(\Omega_1^*, \Omega_2^*, f^*) = \mathbf{argmin}_{\Omega_1, \Omega_2, f: \Omega_1 \rightarrow \Omega_2} \{E_{landmark}(\Omega_1, \Omega_2, f) + E_{intensity}(\Omega_1, \Omega_2, f) + \mathcal{R}(f)\} \quad (1)$$

where $E_{landmark}$ and $E_{intensity}$ are the landmark and intensity mismatching terms respectively. \mathcal{R} is the regularization on f . Note that this problem is different from the conventional registration problem. Apart from the mapping problem, a shape optimization problem has to be solved simultaneously to find the optimal regions Ω_1^* and Ω_2^* .

In this paper, we propose a variational model to solve the above inconsistent surface registration problem through minimizing mapping distortions. We capture the mapping distortions by a geometric quantity, called the *Beltrami coefficient*, from quasi-conformal theory, together with the differential of the mapping. The main idea of the proposed model is to control the angle and scale distortions, while minimizing the landmark and intensity mismatching under the mapping between the partial domains. A splitting method is proposed to iteratively find the optimal corresponding regions on each surfaces and the optimal bijection between them. The incorporation of Beltrami coefficient in our model allows us to conveniently enforce the local bijectivity of the mapping. More specifically, the local bijectivity of the mapping can be easily enforced by a thresholding of the Beltrami coefficient. Numerous tests have been carried out on both synthetic and real data. Experimental results demonstrate the effectiveness of the proposed model to solve the inconsistent surface registration problem.

The contributions of this paper are three-folded.

1. Firstly, we propose to formulate the inconsistent surface registration problem as an optimization problem over the spaces of sub-regions on each surfaces and bijective mappings between them. The regularization of the mapping is based on the differential and the Beltrami coefficient of the mapping from quasiconformal theory, with which the bijectivity of the mapping can be easily enforced.
2. Secondly, we propose an algorithm to obtain a free boundary deformation with controlled scale distortions, whose Beltrami coefficient closely resemble to a prescribed one. This algorithm is useful for solving the optimization problem for inconsistent surface registration in our formulation.
3. Thirdly, a splitting method is proposed to solve the optimization problem, which iteratively searches for the optimal corresponding regions as well as the optimal bijection between them.

The rest of the paper is organized as follows. In section 2, relevant previous works are reviewed. Some basic mathematical background are explained in Section 3. Our proposed model is discussed in details in section 4. Details of the main algorithm to solve the proposed registration model are explained in section 5. Experimental results are shown in section 6. The paper is concluded in section 7.

2 Related works

Surface registration in a non-rigid, deformable setting has been an active and challenging area of research. Since the literature is vast, below we will mention works that are related to ours in terms of the problem setting as well as the techniques deployed, but definitely they will not consist a complete survey.

We approach the inconsistent surface registration problem in 2D parameter domain. Explicitly, we use the conformal, also known as the intrinsic parametrizations [18, 11, 6, 7] of the the surfaces, which faithfully preserve the local geometry of the surfaces. And crucially, we register two inconsistent shapes via optimized deformation in the 2D parametrization domain. Using conformal parametrization is common in recent works on *globally bijective* surface registration possibly with large deformation. For example, for surfaces with prescribed boundary correspondence as in Lam *et al.* [10], for closed surfaces without boundaries as in [5, 15]. Like ours, these works are based on landmark-intensity matching with geometric regularization, where the regularization term is formulated as the local *conformal* or *angular distortion* of the registration map. We refer to [10] and references therein for further related work on the landmark-intensity hybrid registration. However, the local *scale distortion* of the registration map

was not considered by them, mainly because the registration domain are fixed by boundary constraints [10] or in very special forms [5, 15], and thus cannot handle inconsistent shape problems.

In our work we formulate the scale distortion in a uniform framework with the conformal distortion, namely the geometric properties of the mapping differential in quasiconformal theory [3]. In this respect, our work is also closely related to the As-Rigid-As-Possible mesh deformation paradigm [23, 8] and its extensions to allow large non-isometric deformations [13]. Under such a framework geometric smoothness and local bijectivity are non-trivial to achieve and recently many additional optimization methods, *e.g.* [9, 20] are proposed to solve this problem. However, we will show that with conformal parametrization in 2D, it is very easy to achieve geometric smoothness and local bijectivity using the quasiconformal methods. Indeed, our work gathers both the ideas from landmark-intensity registration and mesh deformation modelling to solve the inconsistent shape registration problem possibly with large deformation.

In case the registration map is as simple or close to a global rigid or affine motion, then the inconsistent shape registration problem can also be posed as a fusion problem between surfaces and can be solved by iterative closest point type of methods, please see [22, 12, 2, 4] and the references therein. On the other hand, the feature matching approach is often used in case the registration is allowed to be sparse or possibly locally non-injective. In this regard, methods based on the functional correspondence framework [21, 16] have also been proposed. Differently, we note that our goal is to obtain a locally bijective mapping possibly with large deformation between sub-regions of the surfaces to be registered.

3 Preliminaries on quasiconformal deformations

In this section, we introduce the basic mathematical concepts related to quasiconformal deformations. For our purpose, let X and X' be planar domains in \mathbb{C} of the disk topology equipped with the Euclidean metric. The case of multiply-connected domains is similar. The same concepts can be applied to open surfaces via conformal parametrization.

Consider a diffeomorphism $f : X \rightarrow X'$ between X and X' . This mapping f induces a pullback metric on X , and comparison between this metric and the original Euclidean metric on X reveals geometric properties of f . Quasiconformal theory arises naturally in studying the geometric properties as we now explain.

Consider the pullback metric under f , which can be written as a symmetric positive definite matrix field $H : X \rightarrow \mathbf{S}_{++}$ defined on X . Under this definition, the mapping f satisfies the following nonlinear equation:

$$Df(z)^T Df(z) = H(z).$$

H can be factorized as a product of $\det(Df)$ and a positive definite matrix field Q with unit determinant:

$$H = \det(Df) \cdot Q,$$

Here, we have used the fact that $\det(Df) > 0$ since f is assumed to be a diffeomorphism. This factorization signals a nice linearization of the nonlinear equation we obtained, by multiplying the inverse of $Df(p)^T$ on both sides. More precisely, this will lead to the Beltrami's equation

$$\frac{\partial}{\partial \bar{z}} f(z) = \mu(z) \frac{\partial}{\partial z} f(z),$$

where $\mu = \frac{q_{11} - q_{22} + 2iq_{12}}{q_{11} + q_{22} + 2}$, $Q = (q_{ij})_{1 \leq i, j \leq 2}$ and we use the complex notation $\frac{\partial f}{\partial \bar{z}} = (u_x - v_y)/2 + i(u_y + v_x)/2$, $\frac{\partial f}{\partial z} = (u_x + v_y)/2 + i(-u_y + v_x)/2$. It is easy to check that the diffeomorphism condition implies $|\mu| < 1$ [3]. We call injective solutions to the Beltrami equation with Beltrami coefficient μ quasiconformal mappings. A special case when $\mu = 0$ on X , the equation becomes $\partial_{\bar{z}} f = 0$ and is the well-known Cauchy-Riemann equation. In this case, the mapping f is called a conformal mapping.

The Beltrami coefficient μ is in one-one correspondence to the unit determinant matrix field Q , which encodes the angle distortion of the mapping at the tangent space level. This can be visualized by the fact that quasiconformal mapping maps infinitesimal circles to ellipses. See Figure 1.

The strength of distortion is measured by the condition number of the mapping differential $Df(z)$

$$K(z) = \frac{1 + |\mu(z)|}{1 - |\mu(z)|} = \frac{\sigma_1(Df(z))}{\sigma_2(Df(z))},$$

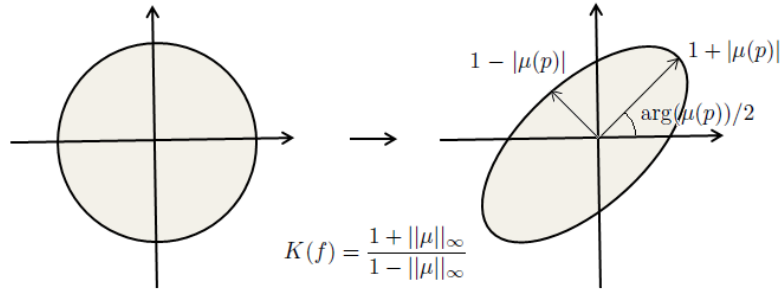


Fig. 1 A quasiconformal mapping maps infinitesimal circles to ellipses. The local geometric distortion under the quasiconformal map can be measured by the Beltrami coefficient.

where $\sigma_1(Df)$ and $\sigma_2(Df)$ is the largest and smallest singular value of the mapping differential Df , which we call the *principal distortions*. One can also observe that as $|\mu|$ tends to 1, the distortion blows up to infinity.

The local area distortion of the mapping is contained inside the Jacobian

$$\det(Df) = \sigma_1(Df) \cdot \sigma_2(Df),$$

which is previously factored out from H and thus not encoded by the Beltrami coefficients. Note that the angle and scale distortions are not independent of each other and they are coupled by a global integrability condition. To be more precise, given Beltrami coefficient μ with $\|\mu\|_\infty < 1$, the equation has unique solution up to post-compositions of conformal mappings [3]. Thus, a unique solution can be obtained, in particular, if the boundary value of the mapping is known, or it can be the *minimal condition* as in the Riemann mapping theorem, namely fixing both the mapping's value as well as its complex derivative at a point.

The above observations about quasiconformal mappings will lead us to a novel free boundary deformation model proposed in this paper, where we take both angle and area distortions into account.

4 Proposed model

In this section, we describe our proposed model for inconsistent surface registration in details. Our strategy is to formulate the problem as an optimization problem to obtain an optimal corresponding regions on each surfaces and the optimal bijection between them. Usually, priori intensity information on the surface, such as the curvature, will be provided. In some situations, corresponding feature landmarks on each surfaces will be delineated. Our variational model can generally be described as finding optimal corresponding regions $\Omega_1^* \subset S_1$, $\Omega_2^* \subset S_2$ and the optimal $f^* : \Omega_1^* \rightarrow \Omega_2^*$ that minimizes:

$$E_{ISR}(\Omega_1, \Omega_2, f) = E_{fid}(\Omega_1, \Omega_2, f) + E_{reg}(f) \quad (2)$$

subject to the constraint that f is in a suitable set \mathcal{A} . E_{fid} is the fidelity term that guides the registration map according to the matching error of intensities on the corresponding regions. E_{reg} is the regularization term for the mapping f that enhances smoothness and reduces local geometric distortions under f . \mathcal{A} is called the *admissible set*, which constrains the mapping f . \mathcal{A} is often defined based on some prescribed requirements according to the problem, such as the landmark constraints.

The above optimization problem can be simplified by conformally parameterizing S_1 and S_2 onto \mathbb{C} . Let $\phi_1 : X \rightarrow S_1$ and $\phi_2 : X' \rightarrow S_2$ be the global conformal parameterizations of S_1 and S_2 respectively. The inconsistent surface registration problem can be reduced to finding the optimal corresponding regions $\Omega_1 := \phi_1^{-1}(\Omega_1)$ and $\Omega_2 := \phi_2^{-1}(\Omega_2)$, as well as the optimal bijection $\hat{f} := \phi_2^{-1} \circ f \circ \phi_1 : \Omega_1 \rightarrow \Omega_2$. As such, we will simply discuss the registration problem between two inconsistent 2D domains $X \subset \mathbb{C}$ and $X' \subset \mathbb{C}$ from now on.

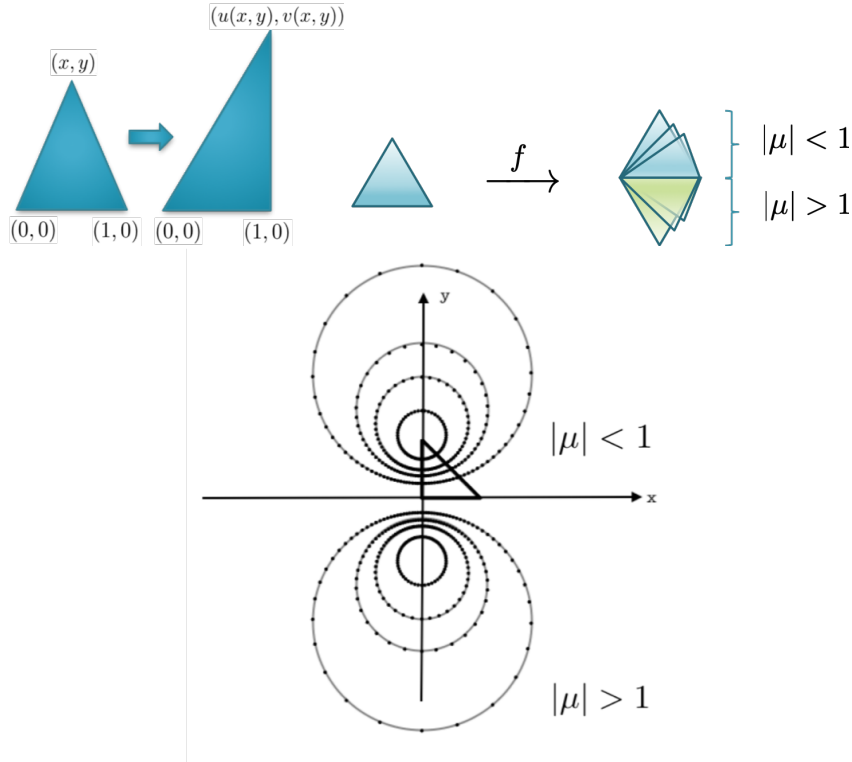


Fig. 2 Deformation of a triangle under various Beltrami coefficients. As shown on the left in the first row, a triangle is being deformed to another triangle, where the two vertices at the base are fixed. The trajectories of the third vertex $(u(x, y), v(x, y))$ under various Beltrami coefficients are shown in the second row. Circles represent the situation when $|\mu| = 1/5, 7/20, 9/20, 3/5, 5/3, 20/9, 20/7, 5$. The Beltrami coefficient can effectively measure local geometric distortions as well as flipping under the deformation, as shown on the right in the first row.

4.1 Choices of E_{fid} and E_{reg}

In this subsection, we discuss our choices of fidelity term E_{fid} , regularization term E_{reg} and admission set A . The fidelity term $E_{fid}(\Omega_1, \Omega_2, f)$ guides the registration map f according to the intensity matching on the corresponding regions Ω_1 and Ω_2 . We consider the following fidelity term:

$$E_{fid}(\Omega_1, \Omega_2, f) = \int_{f(\Omega_1) \cap \Omega_2} (I_1^f - I_2)^2 = \int_{f(X) \cap X'} (I_1^f - I_2)^2, \quad (3)$$

where $I_1 : S_1 \rightarrow \mathbb{R}$ and $I_2 : S_2 \rightarrow \mathbb{R}$ are intensities defined on S_1 and S_2 respectively and $I_1^f := I_1 \circ f^{-1}$ is the deformed image of I_1 under f . It aims to minimize the intensity mismatching under f on the corresponding regions $\Omega_1 \subset X$ and $\Omega_2 \subset X'$. It serves for two purposes. First, it guides the mapping f by matching the intensities as good as possible, so that a meaningful pointwise correspondence between the two surfaces can be obtained. Second, by minimizing over all possible subregions, it optimizes the corresponding subregions using the intensity information defined on each surface. Of course, the first term is equal to 0 in the trivial case when $f(\Omega_1) \cap \Omega_2$ is an empty set. This is the case when the two surfaces are not in correspondence with each other at all. Thus, the regularization term E_{reg} , as well as the landmark constraints, play an important role to avoid this trivial but meaningless case from happening. The domain of integration $f(\Omega_1) \cap \Omega_2$ can be further simplified by observing $f(\Omega_1) \cap \Omega_2 = f(X) \cap X'$. As such, the fidelity term can be simplified to be dependent on the registration map $f : X \rightarrow X'$ only.

As discussed, the choice of the regularization on f is crucial in our model to prevent the undesired trivial case from happening. A natural mapping between two domains should preserve the local geometry as good as possible. Also, the local area distortion or scale distortion under the mapping. We propose a regularization term that handles both sorts of distortions.

The local geometric properties of a diffeomorphic mapping $f : X \rightarrow X'$ is to a large extent determined by the unit determinant component Q of its pullback metric H , thus equivalently its Beltrami co-

efficients. To illustrate this, in Figure 2 we display the distortion effect of different Beltrami coefficients on a triangle. As shown on the left in the first row, a triangle is being deformed to another triangle. For simplicity, we fix the two vertices at the base and let the third vertex $(u(x, y), v(x, y))$ move according to the Beltrami coefficient. The trajectories of the third vertex under different Beltrami coefficients are shown in the second row. When the magnitude of the Beltrami coefficient is fixed, the trajectory is a circle. In the second row, circles represent the situation when $|\mu| = 1/5, 7/20, 9/20, 3/5, 5/3, 20/9, 20/7, 5$. We can see that the deformation of the triangle varies smoothly when the coefficient varies smoothly, and higher smoothness is obtained when the coefficient is closer to zero. Consequently, we expect that smoothness of Beltrami coefficient implies the smoothness of the corresponding solution. This can be made precise via a Schauder estimate for the Beltrami equation, which can be found in [3]. The Beltrami coefficient can effectively measure local geometric distortions as well as flipping under the deformation, as shown on the right in the first row.

From this observation it is natural to consider the following regularization term to find a deformation $f : X \rightarrow \mathbb{C}$ that minimizes:

$$E_{reg}(f) = \frac{1}{2} \int_X \alpha(\mu_0 - \mu(f))^2 + \beta |\nabla \mu(f)|^2, \quad (4)$$

where $\mu(f)$ denotes the Beltrami coefficient of f , μ_0 is a prescribed Beltrami coefficient and $\alpha, \beta \geq 0$ are parameters. Thus, minimizing this energy will promote the smoothness of the mapping g , while trying to preserve a deformation induced by a given Beltrami coefficient μ_0 as much as possible. μ_0 can be prescribed according to the actual situation. In particular, the local geometry can be well preserved if the angle distortions under f are small. As such, we can set μ_0 to be zero if the local geometry has to be preserved. We call such as process to minimize E_{reg} a geometric smoothing process.

4.2 Choice of \mathcal{A}

Other requirements on the registration map may usually be imposed. Mathematically, we need to design a suitable admissible set \mathcal{A} where f should lie in. In our case, we define our admissible set to be the union of three sets of mappings $\mathcal{A} = \mathcal{L} \cup \mathcal{S} \cup \mathcal{B}$. More specifically,

$$\begin{aligned} \mathcal{L} &= \{f : X \rightarrow \mathbb{C} : f(p_i) = q_i, i = 1, 2, \dots, n\}; \\ \mathcal{S} &= \{f : X \rightarrow \mathbb{C} : Df \in \mathcal{M}_{K_1, K_2}\}; \\ \mathcal{B} &= \{f : X \rightarrow \mathbb{C} : \|\mu(f)\|_\infty < 1\}. \end{aligned} \quad (5)$$

where $p_i \in X$ and $q_i \in X'$ are the corresponding landmarks on X and X' respectively, $\mathcal{M}_{K_1, K_2} = \{M : K_2 \leq \sigma_2(M) \leq \sigma_1(M) \leq K_1\}$, $\sigma_1(M)$ and $\sigma_2(M)$ are the larger and smaller singular values of M respectively.

\mathcal{L} encodes the landmark constraints. \mathcal{S} aims to preserve the scale of f as good as possible. Note that the Beltrami coefficient of f encodes the relative strength of stretching effect of f , but not the absolute scale distortion of the mapping. Although the scale can be determined once any of the uniqueness-implying data is applied to solve the equation, such as the boundary value or the minimal condition, there are difficulties with such approaches. In the case of boundary value data, it is often impractical to assume they are available. In the case of minimal condition, how it influences the scale under perturbation of the Beltrami coefficients can be difficult to handle, since one does not have the optimal Beltrami coefficient initially. We thus turn to another aspect of the theory, namely using the singular values of the mapping differential, i.e. principal distortions, for controlling the scale distortion. The singular values of $Df(z)$ contains precise scale information of the mapping f . Controlling their magnitudes with singular value decomposition can be a lot more easier than controlling the Jacobian directly. More specifically, we constrain the singular values of $Df(z)$ such that they are bounded by some prescribed values $K_1 > 0$ and $K_2 > 0$, where $K_1 \leq K_2$. As a result, the local area distortion as captured by $\det(Df(z))$ is bounded by K_1^2 and K_2^2 . The scales of stretching in each principal directions are also bounded by K_1 and K_1 . In particular, the local area is preserved if we set $K_1 = K_2 = 1$.

Finally, \mathcal{B} aims to require the Beltrami coefficient of f to have supreme norm strictly less than 1. It enforces the bijectivity of f .

4.3 Overall model

Our overall inconsistent surface registration model can be summarized as follows. Suppose we are given the prescribed landmark constraints and intensity information on each domains. We look for a registration map $f : X \rightarrow \mathbb{C}$ that minimizes:

$$E_{ISR}(f) = \int_{f(X) \cap X'} (I_1^f - I_2)^2 + \int_X \alpha |\mu(f) - \mu_0|^2 + \beta |\nabla \mu(f)|^2 \quad (6)$$

subject to $f \in \mathcal{A}$.

5 Main algorithm

In this section, we explain our main algorithm to solve the optimization problem (6) in details.

5.1 Projection of f onto \mathcal{S}

Note that in our optimization problem, the registration map f is required to lie in $\mathcal{A} = \mathcal{L} \cup \mathcal{S} \cup \mathcal{B}$. To enforce it, we need projection operators to project a map f to \mathcal{A} . The requirement of $f \in \mathcal{L} \cup \mathcal{B}$ can be taken care of during the projection onto \mathcal{S} and during the minimization process of the regularization term $E_{reg}(f)$, which will be discussed in the next subsection. In this subsection, we discuss the projection of f onto \mathcal{S} in details.

In this work, we consider an iterative scheme to project f onto \mathcal{S} . Given a mapping f , its differential Df may not lie in \mathcal{M}_{K_1, K_2} . We can project Df onto \mathcal{M}_{K_1, K_2} by look for a matrix $\mathcal{P}_{K_1, K_2}(Df)$ that solves the following minimization problem:

$$\mathcal{P}_{K_1, K_2}(Df) = \mathbf{argmin}_{M \in \mathcal{M}_{K_1, K_2}} \|M - Df\|_F^2 \quad (7)$$

Solving this minimization problem is equivalent to finding a projection of $Df(z)$ onto the space of matrices \mathcal{M}_{K_1, K_2} , whose singular values are bounded by K_1 and K_2 . The solution of the problem can be given explicitly as follows.

Theorem 1 *The unique solution of the minimization problem (7) is given by*

$$\mathcal{P}_{K_1, K_2}(Df) = U \begin{pmatrix} \min(\sigma_1(Df), K_1) & \\ & \max(\sigma_2(Df), K_2) \end{pmatrix} V^T,$$

where U, V are the rotation matrices such that $Df = U \begin{pmatrix} \sigma_1(Df) & \\ & \sigma_2(Df) \end{pmatrix} V^T$.

Proof This is related to the general two-sided Procrustes problem. Suppose X_1 and X_2 are two $n \times n$ matrices. $X_1 = U_1 \Sigma_1 V_1^T$ and $X_2 = U_2 \Sigma_2 V_2^T$ are the singular value decompositions of X_1 and X_2 respectively. Consider

$$E_{P1}(Q_1, Q_2) = \|Q_1^T X_1 Q_2 - X_2\|_F^2,$$

where Q_1 and Q_2 are $n \times n$ orthogonal matrices. Then, the minimizer of E_{P1} satisfies:

$$U_1 = Q_1 U_2 \Pi \text{ and } V_1 = Q_2 V_2 \Pi, \quad (8)$$

where Π is the permutation matrix that minimizes $Tr(\Sigma_2 \Pi \Sigma_1 \Pi)$ (see p.89-90 in [20]).

We now consider our original minimization problem (7). Let $M = U_M \Sigma V_M^T$ be the singular value decomposition of M . Then, we observe that:

$$\|U \begin{pmatrix} \sigma_1(Df) & \\ & \sigma_2(Df) \end{pmatrix} V^T - U_M \Sigma V_M^T\|_F^2 = \left\| \begin{pmatrix} \sigma_1(Df) & \\ & \sigma_2(Df) \end{pmatrix} - Q_1^T \Sigma Q_2 \right\|_F^2,$$

where $Q_1 = U_M^T U$ and $Q_2 = V_M^T V$ are orthogonal matrices. Thus, the minimization problem (7) is equivalent to minimizing:

$$E_{P2}(Q_1, \Sigma, Q_2) = \left\| \begin{pmatrix} \sigma_1(Df) & \\ & \sigma_2(Df) \end{pmatrix} - Q_1^T \Sigma Q_2 \right\|_F^2.$$

Fixing a diagonal matrix Σ , we consider the minimization problem over (P, Q) of $E_{P2}(P, \Sigma, Q)$. Then, the minimizer must satisfy $I = P\Pi$ and $I = Q\Pi$ according to (8). Thus, for any orthogonal matrices Q_1 and Q_2 together with any diagonal matrix Σ ,

$$\begin{aligned} E_{P2}(Q_1, \Sigma, Q_2) &= \left\| \begin{pmatrix} \sigma_1(Df) & \\ & \sigma_2(Df) \end{pmatrix} - Q_1^T \Sigma Q_2 \right\|_F^2 \\ &\geq \left\| \begin{pmatrix} \sigma_1(Df) & \\ & \sigma_2(Df) \end{pmatrix} - \Pi \Sigma \Pi \right\|_F^2 \\ &\geq \left\| \begin{pmatrix} \sigma_1(Df) & \\ & \sigma_2(Df) \end{pmatrix} - \bar{\Sigma} \right\|_F^2 \\ &= E_{P2}(I, \bar{\Sigma}, I), \end{aligned}$$

where $\bar{\Sigma}$ is the minimizer of $\left\| \begin{pmatrix} \sigma_1(Df) & \\ & \sigma_2(Df) \end{pmatrix} - D \right\|_F^2$ over all diagonal matrix D with diagonal entries bounded by K_1 and K_2 . Obviously, $\bar{\Sigma}$ can be written explicitly as:

$$\bar{\Sigma} = \begin{pmatrix} \min(\sigma_1(Df), K_1) & \\ & \max(\sigma_2(Df), K_2) \end{pmatrix}.$$

We conclude that: $M = UI\bar{\Sigma}IV^T = U\bar{\Sigma}V^T$ is the minimizer of the problem (7). This completes the proof.

We call \mathcal{P}_{K_1, K_2} the projection operator of a matrix onto the space \mathcal{M}_{K_1, K_2} . In this way we can effectively control the scaling effect of the mapping at each point. For simplicity we shall use K_1, K_2 uniformly on the domain, though other choices are clearly possible. We next look for a mapping $g : X \rightarrow \mathbb{C}$, whose differential is closely resemble to $\mathcal{P}_{K_1, K_2}(Df)$:

$$E_{\mathcal{P}}(g) = \int_X \|Dg - \mathcal{P}_{K_1, K_2}(Df)\|_F^2. \quad (9)$$

We can separate the above minimization problem for each coordinate u, v of g , and therefore we are left with two Poisson equations as their Euler-Lagrange equations:

$$\begin{cases} -\Delta u &= -\nabla \cdot w_1 \\ -\Delta v &= -\nabla \cdot w_2 \end{cases}, \quad (10)$$

where $\mathcal{P}_{K_1, K_2}(Df) = (w_1, w_2)$. The landmark constraints can be incorporated here via back substitution into (10). In this way, f is constrained to lie in \mathcal{L} . We repeat this procedure iteratively. More precisely, given a map $f^{(i)}$, we compute $\mathcal{P}_{K_1, K_2}(Df^{(i)})$. We then compute $f^{(i+1)}$ that minimizes $E_{\mathcal{P}}$. The iterative algorithm can be summarized in Algorithm 1.

Algorithm 1 Projection onto \mathcal{S}

Inputs: null deformation (identity mapping) $f^{(1)}$, iteration number N , bounds on singular values $0 < K_2 \leq K_1$, landmark correspondences (p_i, p'_i) .

Output: deformed mapping $f^{(N)}$.

for $i = 1, \dots, N$ **do**

 Compute $Df^{(i)}$ and its singular value decomposition on each triangular face.

 Compute $W^{(i)} = \mathcal{P}_{K_1, K_2}(Df^{(i)})$ on each triangular face.

 Solve equations (10) with landmark constraints to get $f^{(i+1)}$.

end for

5.2 Linear Beltrami Solver

Solving Beltrami equation with given coefficient function μ is central to our optimization problem, in which boundary datum is assumed. Solvers of the equation, with or without boundary datum, are developed in the previous work [14, 19], and therefore we briefly only introduce the main components here and refer the reader to the references for details.

The key is to note the relation between the Beltrami equations and *div*-type second order elliptic systems. In our case, we decouple the complex equation into its real and imaginary parts u and v respectively, and solve the following system of equations with Dirichlet boundary condition

$$\begin{cases} -\nabla \cdot (A\nabla u(z)) = 0 & \text{in } \text{int}(X) \\ -\nabla \cdot (A\nabla v(z)) = 0 & \text{in } \text{int}(X) \\ u = u_0 & \text{on } \partial X \\ v = v_0 & \text{on } \partial X \end{cases} \quad (11)$$

where $A = \frac{1}{1-|\mu|^2} \begin{bmatrix} (\rho-1)^2 + \tau^2 & -2\tau \\ -2\tau & (1+\rho)^2 + \tau^2 \end{bmatrix}$, $\mu = \rho + i\tau$, and $\text{int}(X)$ is the interior of X . In practice, the operator $\nabla \cdot (A\nabla)$ is discretized using linear finite element method on triangular meshes, which has the same form with the famous cotangent formula for the discrete Laplacian [19]. We call such a solver the **Linear Beltrami Solver**. We also denote the reconstructed quasiconformal map f from μ by $f = \mathbf{LBS}(\mu, \{(p_i, q_i)\}_{i=1}^L)$, where $\{(p_i, q_i)\}_{i=1}^L$ denotes the prescribed corresponding landmark constraints.

5.3 Free boundary quasiconformal deformation

To solve the registration model (6), we need an algorithm to obtain a free boundary deformation with controlled distortions, whose Beltrami coefficient closely resemble to a prescribed one. The free boundary deformation does not require the source domain to be mapped to another target domain with fixed geometry. As such, surface registration problem, of which a natural bijection between two surfaces does not exist, can be handled using our formulation.

In this subsection, we discuss an iterative scheme to obtain a free boundary quasiconformal deformation. With a prescribed Beltrami coefficient μ_0 , our strategy is to iteratively adjust the quasiconformal map to reduce the smoothing energy $E_{reg}(f)$. Suppose a quasiconformal map $f^{(k)}$ is obtained at the k -th iteration. We proceed to update it to $f^{(k+1)}$ according to the gradient descent direction of $E_{reg}(f)$.

Firstly, it is desirable to obtain a quasiconformal map with a controlled scale distortion. It can be achieved by requiring the quasiconformal map to lie in \mathcal{S} . Hence, the projection step as described in subsection (5.1) is applied on $f^{(k)}$ to obtain a new map $g^{(i,1)}$.

Secondly, we proceed to minimize the regularization term. We call such a process a *geometric smoothing step*. Denote the Beltrami coefficient of $g^{(i,1)}$ by $\mu_{g^{(i,1)}}$. To enforce $g^{(i,1)} \in \mathcal{B}$, we require that the supreme norm of the Beltrami coefficient is strictly less than 1. It ensures the bijectivity of the registration map. We apply the following simple thresholding method:

$$\mu'_{g^{(i,1)}}(z) = \begin{cases} \mu_{g^{(i,1)}} & \text{if } |\mu_{g^{(i,1)}}(z)| < 1 \\ 0 & \text{otherwise} \end{cases}. \quad (12)$$

Descending E_{reg} can be achieved as follows. By computing the gradient descent direction of E_{reg} , we can update $\mu'_{g^{(i,1)}}(z)$ via the following iterative scheme:

$$\nu^{(j+1)} = (1 - \alpha)\nu^{(j)} + \alpha\mu_0 + \beta\Delta\nu^{(j)}, \quad (13)$$

where Δ is the Laplace-Beltrami operator of the domain and $\nu^{(0)} = \mu'_{g^{(i,1)}}$. We can keep the process for few (say M_2) iterations, to minimize E_{reg} . The associated registration map can be reconstructed by Linear Beltrami solver to obtain a new map $g^{(i,2)}$ with Dirichlet boundary condition given by $g^{(i,1)}$, subject to the prescribed landmark constraints that $g^{(i,2)}(p_i) = q_i$ for $i = 1, 2, \dots, n$. We keep this process for M_1 iterations to obtain $g^{(i, M_1)}$ and set $f^{(k+1)} = g^{(i, M_1)}$. We run the above iterations to obtain a sequence of quasiconformal maps $\{f^{(k)}\}_{k=1}^N$.

We also denote the free boundary quasiconformal map f from μ_0 by $f = \mathcal{FD}(\mu_0, \{(p_i, q_i)\}_{i=1}^n)$, where $\{(p_i, q_i)\}_{i=1}^n$ denotes the prescribed corresponding landmark constraints. We remark that our algorithm to obtain the free boundary deformation requires only two landmark constraints. That is, $n = 2$. The overall algorithm can be summarized in Algorithm 2.

Algorithm 2 Free boundary quasiconformal deformation

Inputs: null deformation (identity mapping) $f^{(1)}$, overall iteration number N ; Projection step iteration number N_1 , bounds on singular values $0 < K_2 \leq K_1$, landmark correspondences $\{(p_i, q_i)\}_{i=1}^n$; smoothing parameters $\alpha, \beta > 0$ and smoothing step iteration numbers M_1, M_2 .

Output: Optimal free boundary quasiconformal deformation $f^{(N)}$.

for $i = 1, \dots, N$ **do**

for $l = 1, \dots, N_1$ **do**

 Compute $Df^{(i)}$ and its singular value decomposition on each triangular face.

 Compute $W^{(i)} = \mathcal{P}_{K_1, K_2}(Df^{(i)})$ on each triangular face.

 Solve equations (10) with landmark constraints to get $g^{(i,1)}$.

end for

for $j = 1, \dots, M_1$ **do**

 Compute the Beltrami coefficients of $g^{(i,j)}$ and applying the thresholding (18).

for $k = 1, \dots, M_2$ **do**

 Run the iteration according to (13).

end for

 Set $\nu = \nu^{(M_2+1)}$.

 Set $g^{(i,j+1)} = \mathbf{LBS}(\nu, \{(p_i, q_i)\}_{i=1}^L)$.

end for

 Set $f^{(i+1)} = g^{(i, M_1)}$.

end for

5.4 A splitting scheme for inconsistent surface registration model (6)

In this subsection, we discuss an iterative scheme to solve the optimization problem (6). Our strategy is to minimize E_{ISR} alternatively. We look for a descent direction to minimize the regularization term E_{fid} and then a descent direction to minimize the fidelity term E_{reg} . Suppose a mapping $f^{(k)}$ is obtained at the k -th iteration. We proceed to update $f^{(k)}$ to obtain a new mapping $f^{(k+1)}$. In essence, the iterative algorithm is a modification of Algorithm 2. It employs the idea of Algorithm 2 to obtain a free boundary quasiconformal deformation. And Algorithm 2 is modified by adding a substep to minimize the intensity mismatching to solve the inconsistent surface registration problem.

Again, to enforce the registration map to lie in \mathcal{S} , the projection step as described in subsection 5.1 is carried out to obtain a new map $g^{(i,1)}$.

To minimize E_{ISR} , we first consider the descent direction of E_{fid} . Recall that our intensity registration problem aims to minimize the following loss function

$$\int |I_X \circ f^{-1} - I_Y|^2 \cdot \chi_{f(X) \cap Y} dx dy,$$

where χ_A denotes the indicator function of the set A .

Given fixed $g^{(i,1)}(X) \cap Y$, we can minimize the intensity mismatching term by using the gradient descent method. Write $g^{(i,1)} = \text{Id} - \mathbf{u}$, the intensity mismatching term can be reformulated as $\int_{g^{(i,1)}(X) \cap Y} |I_X - I_Y(\text{Id} - \mathbf{u})|^2 dx dy$. Minimizing this energy using gradient descent may lead to unstable and non-diffeomorphic solutions. Recall that our algorithm aim to obtain a diffeomorphic registration. To alleviate this issue, a regularization term is often introduced [17, 24]:

$$E(\mathbf{u}) = \int_{g^{(i,1)}(X) \cap Y} |I_X - I_Y(\text{Id} - \mathbf{u})|^2 + \frac{\sigma_i^2}{\sigma_T^2} R(\mathbf{u}), \quad (14)$$

where σ_i and σ_T are some constants related to the intensity difference and the deformation respectively. By considering the Taylor's expansion of $I_Y(\text{Id} - \mathbf{u})$ and defining $R(\mathbf{u}) = \|\mathbf{u}\|^2$,

$$E(\mathbf{u}) \approx \|I_X - I_Y + \mathbf{u}^T \nabla I_Y\|_2^2 + \frac{\sigma_i^2}{\sigma_T^2} \|\mathbf{u}\|_2^2. \quad (15)$$

By taking gradient on both sides with respect to u , we obtain

$$\nabla E(\mathbf{u}) = 2(I_X - I_Y + \mathbf{u}^T \nabla I_Y) \nabla I_Y + 2 \frac{\sigma_i^2}{\sigma_T^2} \mathbf{u}. \quad (16)$$

$\nabla E(\mathbf{u})$ gives us the descent direction to update $g^{(i,1)}$, such that the fidelity (intensity mismatching) term can be reduced. As a result, we will obtain a vector field $\mathbf{V} = (V_1, V_2)$ that gives a new map $\tilde{g} = \text{Id} + \mathbf{V}$. Its associated Beltrami coefficient $\mu_{\tilde{g}}$ is given by

$$\mu_{\tilde{g}} = \frac{(\frac{\partial V_1}{\partial x} - \frac{\partial V_2}{\partial y}) + i(\frac{\partial V_2}{\partial x} + \frac{\partial V_1}{\partial y})}{(2 + \frac{\partial V_1}{\partial x} + \frac{\partial V_2}{\partial y}) + i(\frac{\partial V_2}{\partial x} - \frac{\partial V_1}{\partial y})}. \quad (17)$$

To enforce the registration map lies in \mathcal{B} , we require that the supreme norm of the Beltrami coefficient is strictly less than 1. It ensures the bijectivity of the registration map. We again apply the following simple thresholding method:

$$\mu'_{\tilde{g}}(z) = \begin{cases} \mu_{\tilde{g}} & \text{if } |\mu_{\tilde{g}}(z)| < 1 \\ 0 & \text{otherwise} \end{cases}. \quad (18)$$

After that, we proceed to minimize the regularization term. Descending E_{reg} can be achieved using the equation (13) as described in subsection 5.3. This gives an updated Beltrami coefficient ν .

The associated quasiconformal map can be reconstructed by Linear Beltrami Solver to obtain $g^{(k,2)} = \mathbf{LBS}(\nu)$, subject to the prescribed landmark constraints. We repeat the process to iteratively minimize E_{ISR} for M iterations and set $f^{(k+1)} = g^{(i,M)}$.

The main algorithm can now be summarized as follows.

Algorithm 3 Registration on inconsistent domains

Inputs: null deformation (identity mapping) $f^{(1)}$, overall iteration number N ; free boundary subproblem iteration number N_1 , bounds on singular values $0 < K_2 \leq K_1$, landmark correspondences (p_i, p'_i) ; Demon's algorithm parameters; smoothing parameters $\alpha, \beta > 0$ and subproblem iteration numbers M_1, M_2 .

Output: optimal deformation $f^{(N)}$ given landmarks and intensities in the sense of ??

for $i = 1, \dots, N$ **do**

for $l = 1, \dots, N_1$ **do**

 Compute $Df^{(i)}$ and its singular value decomposition on each triangular face.

 Compute $W^{(i)} = \mathcal{P}_{K_1, K_2}(Df^{(i)})$ on each triangular face.

 Solve equations (10) with landmark constraints to get $g^{(i,1)}$.

end for

for $j = 1, \dots, M$ **do**

 Obtain a vector field $V^{(j)}$ on $g^{(k,j)}(X) \cap Y$ by matching intensities $\chi_{g^{(i,j)}(X) \cap Y} I_X \circ (g^{(i,j)})^{-1}$ and $\chi_{g^{(i,j)}(X) \cap Y} \cdot I_Y$ according to Equation (16).

 Apply $V^{(j)}$ to $g^{(k,j)}$ to get new registration map \tilde{g} .

 Compute the Beltrami coefficients of \tilde{g} and applying the thresholding (18).

 Run the iteration according to (13) to iteratively minimize E_{reg} to get an update Beltrami coefficient ν .

 Solve the Beltrami equation using the updated coefficient to get $g^{(i,j+1)}$.

end for

 Set $f^{(i+1)} = g^{(i,M)}$.

end for

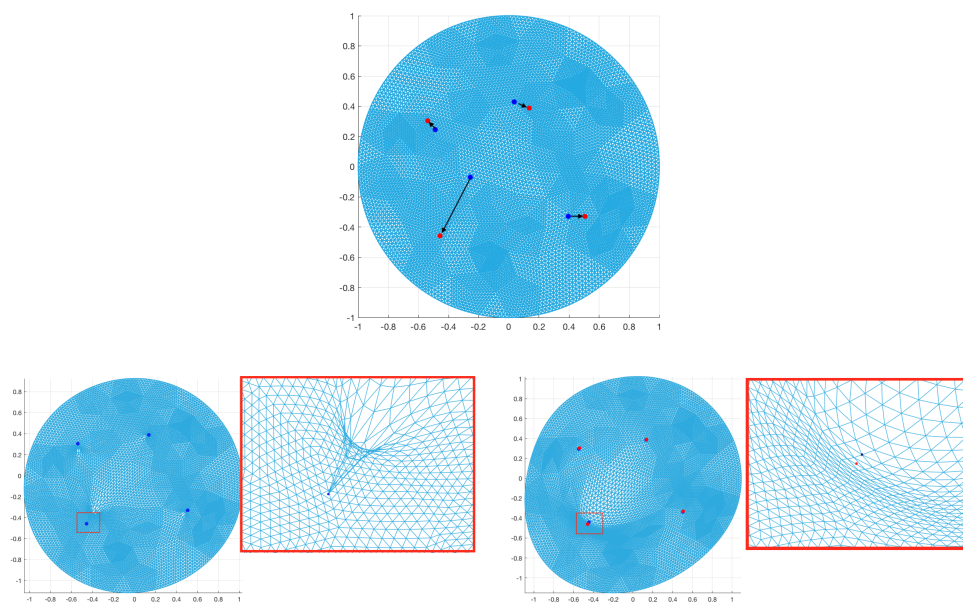


Fig. 3 Effect of the geometric smoothing. The first row shows the input mesh. The landmark correspondences are displayed. We deform the input mesh so that the blue landmarks are matched to the red landmarks, using our proposed free boundary quasiconformal deformation algorithm. In the second row, the result on the left is obtained without geometric smoothing. The result on the right shows the output of the algorithm with geometric smoothing.

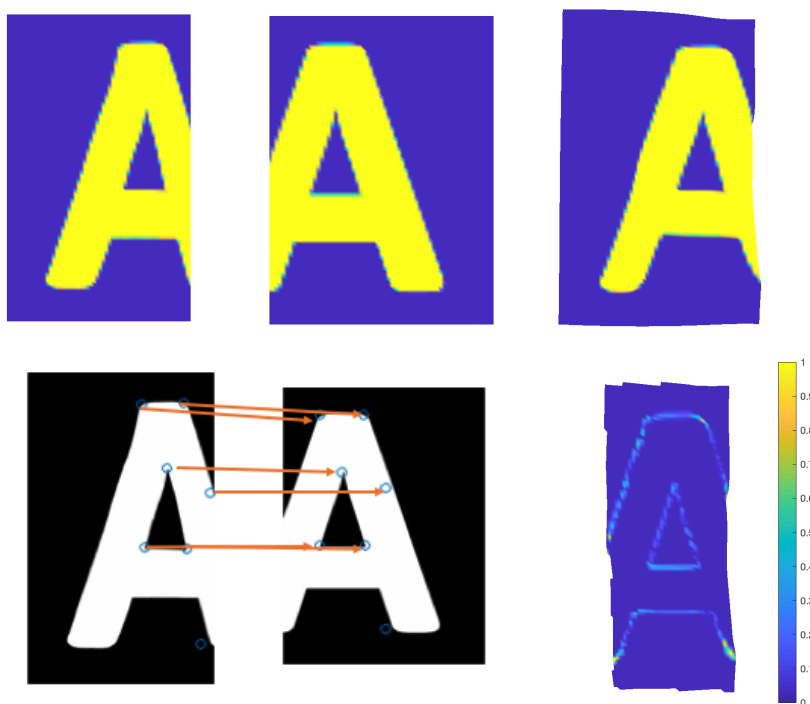


Fig. 4 Result of the inconsistent image registration experiment in Example 2. The left in the first row shows the input moving image. The middle in the first row shows the input static image. Our goal is to register the left taller “A” to the middle wider “A”. The left in the second row shows the prescribed landmark correspondences. The registered image from the moving image is shown on the right in the first row. The right in the second row shows the absolute difference in intensity after registration.

6 Experimental results

6.1 Synthetic numerical experiments

In this subsection, we test the performance of our proposed algorithms on two synthetic examples.

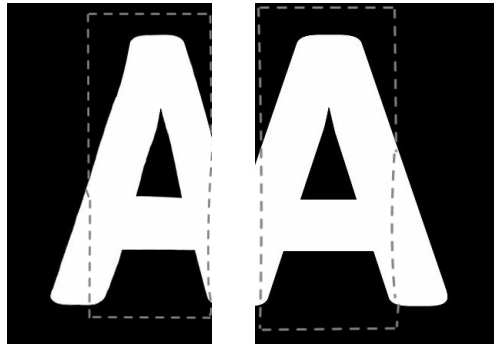


Fig. 5 Corresponding regions on the moving and static images. The region bounded by the dotted curve on left shows the corresponding region on the moving image. The region bounded by the dotted curve on the right shows the corresponding region on the target image.

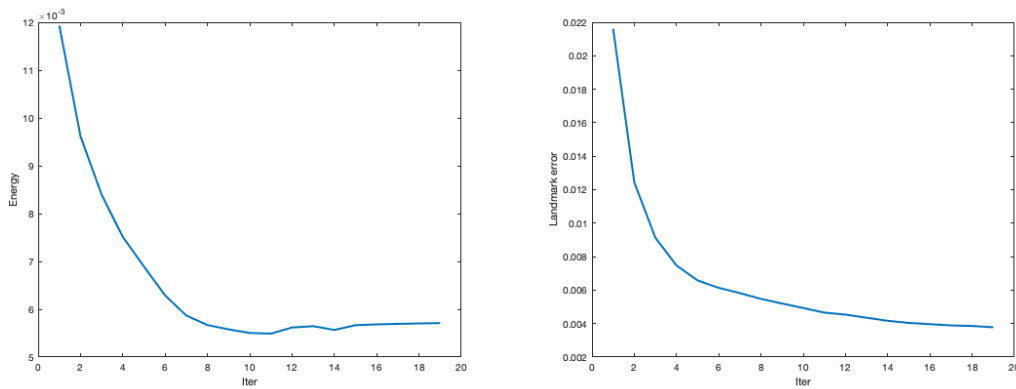


Fig. 6 Energy and landmark error plots for the image registration experiment against iteration number. Energy is averaged per triangular face. The left shows the overall energy versus iterations. The right shows the landmark mismatching error versus iterations.

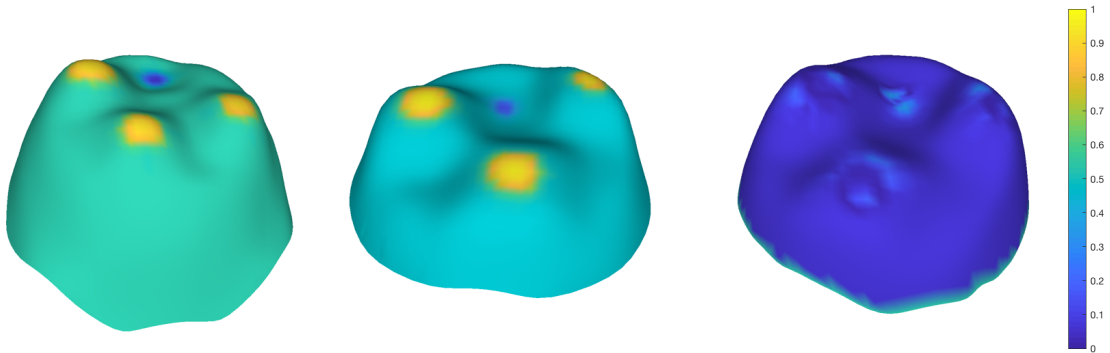


Fig. 7 Surface registration for a pair of inconsistent tooth surfaces in Example 3. The left shows the input moving tooth surface. The middle shows the target static tooth surface. The right shows the difference of intensities on the registered surface.

Example 1 (*The Effect of geometric smoothing*): In this example, we test our algorithm for free boundary quasiconformal deformation (Algorithm 2), given landmark constraints as shown in the first row of Figure 3. We have chosen $\alpha = \beta = 0.1$ and smoothing steps $M_1 = 30, M_2 = 10$. Bounds on singular values are chosen to be $K_1 = 5, K_2 = 0.2$. The result without geometric smoothing (that is, setting $M_1 = M_2 = 0$) is shown on the left in the second row, where one can clearly observe flipping and non-smooth singularities around the landmark points. The result with geometric smoothing in the third row, where the local deformations are well propagated around the landmark points and the obtained deformation is smooth. This shows the necessity and effectiveness of the geometric smoothing scheme.

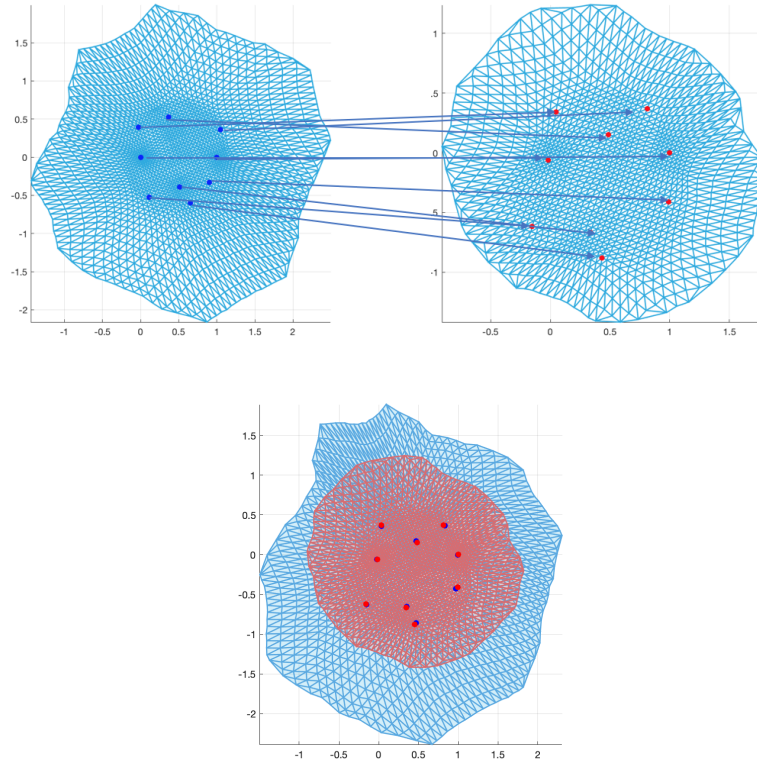


Fig. 8 The left in the first row shows the conformal parametrization of the moving tooth surface in Example 3. The right in the second row shows the conformal parametrization of the static tooth surface. The landmark correspondences in the 2D parameter domains are also displayed. The registration result in the 2D domain is shown in the second row. The blue mesh is transformed mesh from the moving mesh under the registration map. The red mesh is the 2D mesh of the target surface under the conformal parametrization.

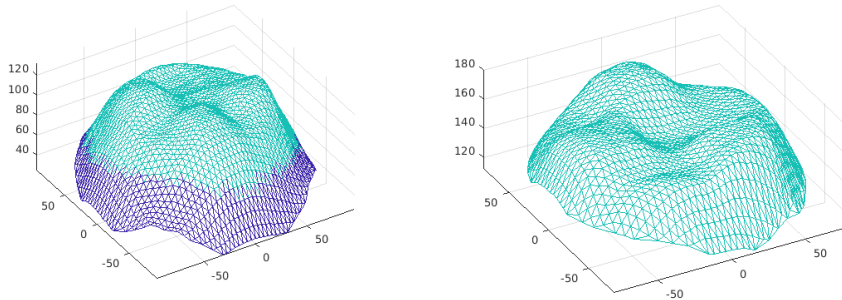


Fig. 9 Corresponding regions on the moving and static tooth surfaces in Example 3. The green region on left shows the corresponding region on the moving tooth surface. The green region on the right shows the corresponding region on the target tooth surface.

Example 2 (*Registration of a pair of images*): In this example, we test our intensity registration model (Algorithm 3) on an inconsistent pair of images of the letter “A”. In Figure 4, the left on the first row shows the input images with their intensities to be matched, where the one on the left is the moving domain. Our goal is to register the left taller “A” to the middle wider “A”. The given landmark correspondences are shown on the left in the second row. In this example, we set $\alpha = 0.01, \beta = 0.01$, smoothing steps $M_1 = 1, M_2 = 10$; bounds $K_1 = 1.4, K_2 = 0.2$; free boundary subproblem for $N_1 = 1$ iterations; intensity subproblem for 20 iterations and overall iteration $N = 20$. The registered image from the moving image is shown on the right in the second row. It closely resembles to the target static image. The absolute difference in intensity after registration is shown on the right in the first row. This

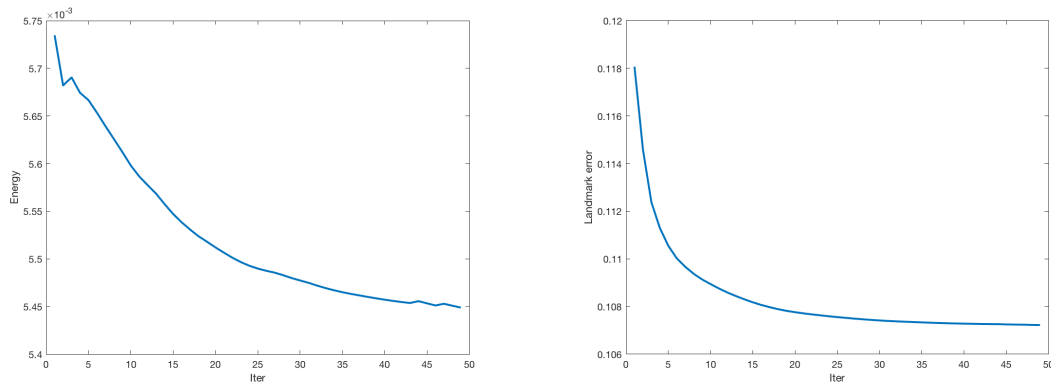


Fig. 10 Energy and landmark error plots for the teeth experiment in Example 3 against iteration number. Energy is averaged per face. The left shows the overall energy versus iterations. The right shows the landmark mismatching error versus iterations.

experimental result demonstrates that our algorithm is effective in finding an accurate registration map matching the intensities as well as finding the corresponding regions on the images.

We also display the energy plot against the iteration number averaged per face of the mesh on the left of Figure 6, and the landmark error plot on the left. We can see that the algorithm successfully reduces the intensity and landmark mismatching errors.

6.2 Experiments on surfaces

In this subsection, we test our registration model on surfaces.

Example 3 (*Registration of a pair of synthetic teeth surfaces*): In this example, we test the registration model on an inconsistent pair of tooth surfaces. The two surfaces are not bijectively corresponding to each others. Only a partial subset of the source surface is in correspondence with a subset of the target surface.

In Figure 7, the first and second columns shows the input surfaces with their curvatures to be matched, where the one on the left is the moving surface. We first perform conformal flattening [11] of the two 3D meshes into 2D, as shown in the first row in Figure 8. The landmark correspondences in the 2D parameter domains are also displayed. In this example, we have used $\alpha = 0.01, \beta = 0.1$, smoothing steps $M_1 = 1, M_2 = 10$; bounds $K_1 = 1.2, K_2 = 0.8$; free boundary subproblem for $N_1 = 5$ iterations; intensity subproblem for 10 iterations and overall iteration $N = 50$. The registration result is shown in the last column of Figure 7. It is the registered surface from the moving surface to the target static surface. The colormap on the surface is given by the curvature mismatching error. Note that the mismatching error is small, indicating the curvatures are accurately matched. The registration result in the 2D domain is shown in the second row of Figure 8. The blue mesh is transformed mesh from the moving mesh under the registration map. The red mesh is the 2D mesh of the target surface under the conformal parametrization. The intersection region of the two meshes is the region of correspondence amongst the two tooth surfaces.

We also display the energy plot against iteration number averaged per face of the mesh on the left of Figure 10, and the landmark error plot on the left. We can see that the algorithm successfully reduces the intensity and landmark matching errors.

Example 4 (*Registration of partial tooth surfaces*): Here, we test our registration model on another inconsistent pair of teeth. In Figure 11, the first and second columns show the moving tooth surface and the target static tooth surface respectively. The two surfaces are obviously not bijectively corresponding to each others. Again, our goal is to simultaneously look for the corresponding regions on each surface as well as the registration map between them. The colormaps on each surfaces are given by their curvatures, which are to be matched using our registration algorithm. As before we first perform conformal flattening [11] of the two surface meshes into 2D, as shown in the first row in Figure 12. The landmark correspondences in the 2D parameter domains are also shown. In this example, we have

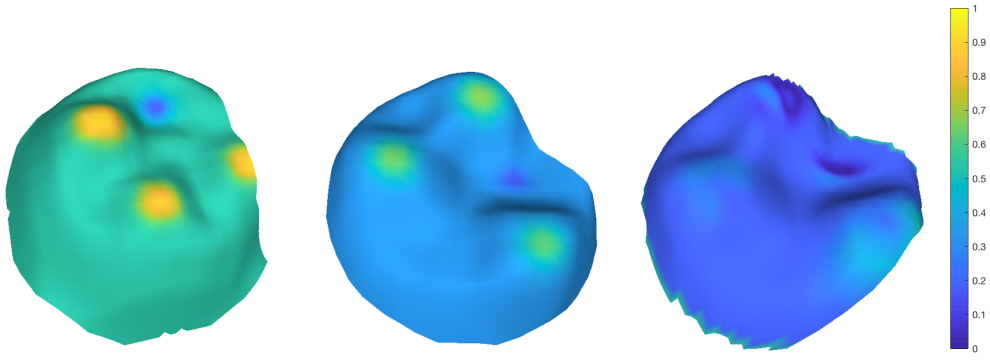


Fig. 11 Surface registration for another pair of inconsistent tooth surfaces in Example 4. The left shows the input moving tooth surface. The middle shows the target static tooth surface. The right shows the difference of intensities on the registered surface.

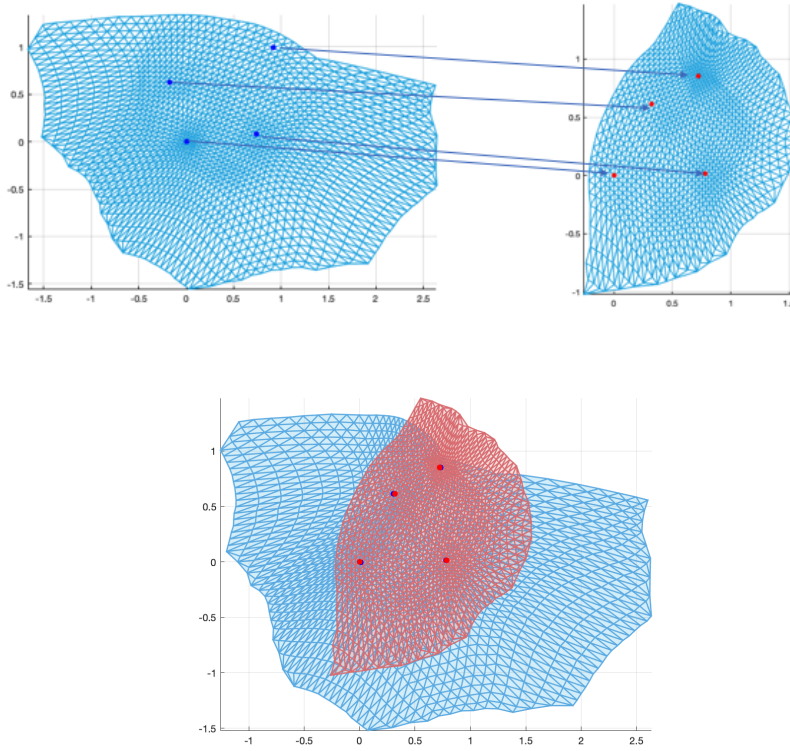


Fig. 12 The first row shows the conformal parametrizations of the moving and static tooth surfaces in Example 4 respectively. The landmark correspondences in the 2D parameter domains are also displayed. The registration result in the 2D domain is shown in the second row. The blue mesh is transformed mesh from the moving mesh under the registration map. The red mesh is the 2D mesh of the target surface under the conformal parameterization. The intersection represents the corresponding region.

used $\alpha = 0.06, \beta = 0.11$, smoothing steps $M_1 = 1, M_2 = 5$; bounds $K_1 = 1.3, K_2 = 0.4$; free boundary subproblem for $N_1 = 1$ iterations; intensity subproblem for 1 iterations and overall iteration $N = 50$. The registration result is shown in the last column of Figure 11. It is the registered surface from the moving surface to the target static surface. The colormap on the surface is given by the curvature mismatching error. Note that the mismatching error is small, indicating the curvatures are accurately matched. The registration result in the 2D domain is shown in the second row of Figure 12. The blue mesh is transformed mesh from the moving mesh under the registration map. The red mesh is the 2D mesh of the target surface under the conformal parameterization. The intersection region of the two

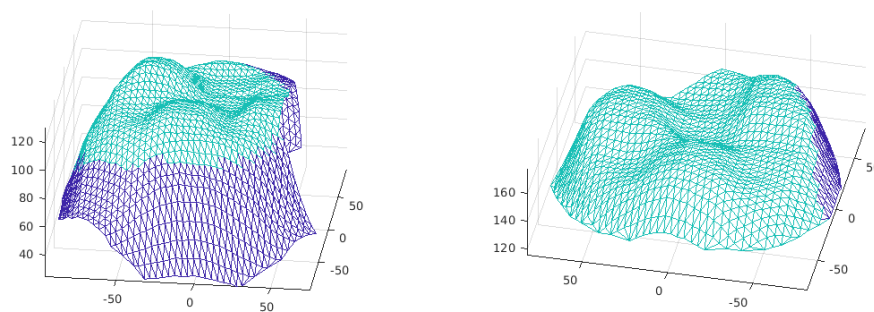


Fig. 13 Corresponding regions on the moving and static tooth surfaces in Example 4. The green region on left shows the corresponding region on the moving tooth surface. The green region on the right shows the corresponding region on the target tooth surface.

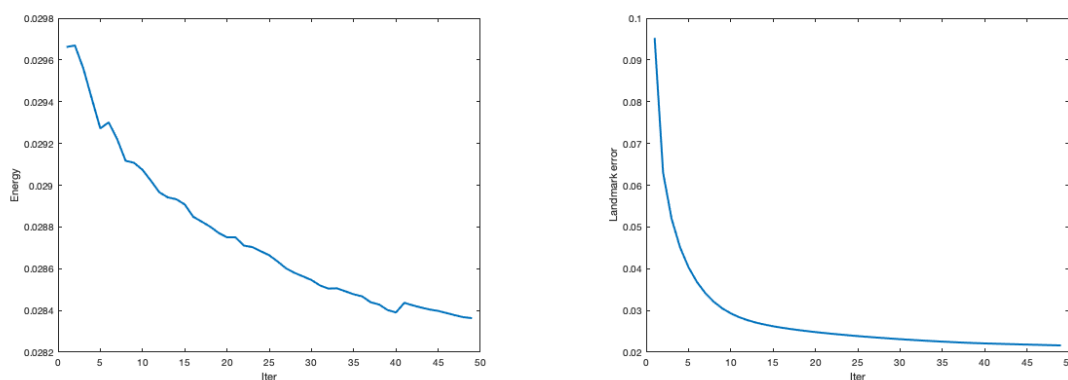


Fig. 14 Energy and landmark error plots for the tooth surface experiment in Example 4 against iteration number. Energy is averaged per face. The left shows the overall energy versus iterations. The right shows the landmark mismatching error versus iterations.

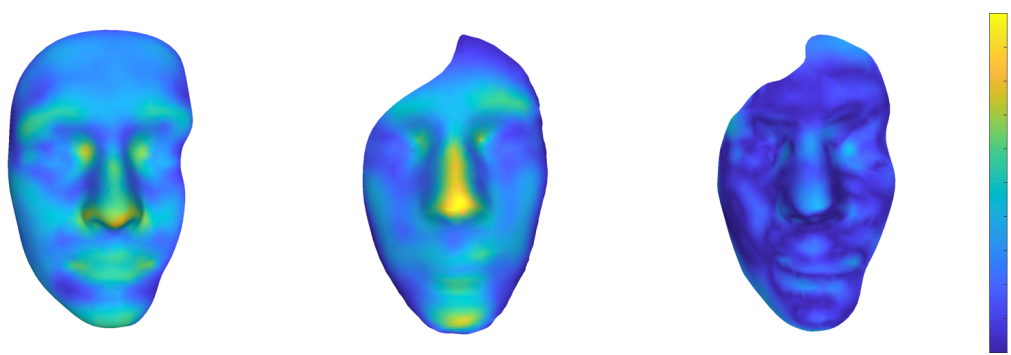


Fig. 15 Surface registration for a pair of inconsistent human faces in Example 5. The left shows the input moving surface. The middle shows the target static surface. The right shows the difference of intensities on the registered surface.

meshes is the region of correspondence amongst the two tooth surfaces. We also display the energy plot against iteration number averaged per face of the mesh on the left of Figure 14, and the landmark error plot on the left. We can observe that the algorithm successfully reduces the intensity and landmark matching errors.

Example 5 (Registration of a pair of human faces): In this example, we test our registration method on a pair of inconsistent human faces, which are obtained from FIDENTIS 3D Face Database [1]. The first and second columns in Figure 15 show the moving human face and the target static human face respectively. The colormaps on each surfaces are given by their mean curvatures. The two surfaces are not bijectively corresponding to each others. As before, we first perform conformal flattening [11] of the

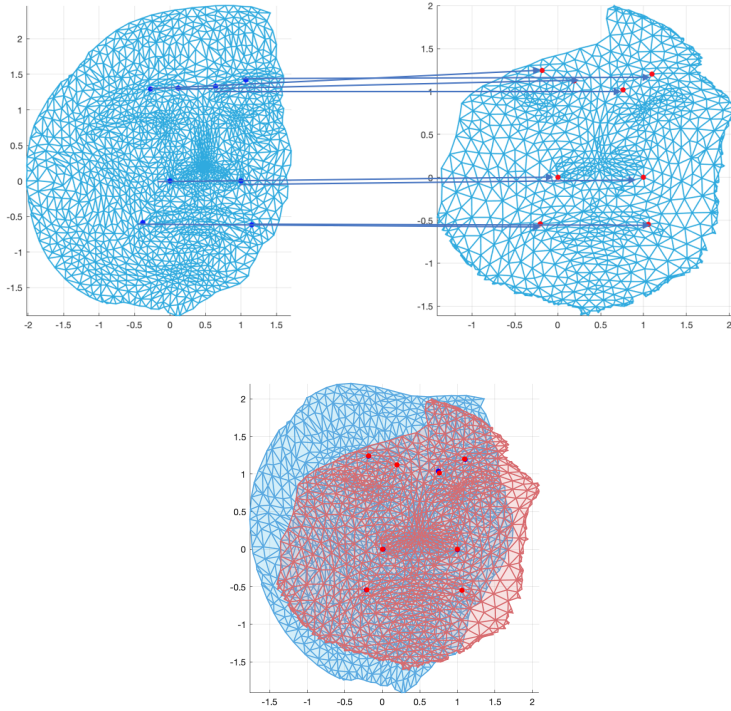


Fig. 16 The first row shows the conformal parametrizations of the moving and static human faces in Example 5 respectively. The landmark correspondences in the 2D parameter domains are also displayed. The registration result in the 2D domain is shown in the second row. The blue mesh is transformed mesh from the moving mesh under the registration map. The red mesh is the 2D mesh of the target surface under the conformal parametrization.

two surface meshes into 2D, as shown in the first row of Figure 16. The landmark correspondences in the 2D parameter domains are also shown. In this example, we have used $\alpha = 0.1, \beta = 0.1$, smoothing steps $M_1 = 1, M_2 = 10$; bounds $K_1 = 1.2, K_2 = 0.8$; free boundary subproblem for $N_1 = 5$ iterations; intensity subproblem for 10 iterations and overall iteration $N = 50$. The registration result is shown in the last column of Figure 15. It is the registered surface from the moving surface to the target static surface. The colormap on the surface is given by the curvature mismatching error. Note that the mismatching error is small, indicating the curvatures are accurately matched. The registration result in the 2D domain is shown in the second row of Figure 16. The blue mesh is transformed mesh from the moving mesh under the registration map. The red mesh is the 2D mesh of the target surface under the conformal parameterization. The intersection region of the two meshes is the region of correspondence amongst the two human faces. We also display the energy plot against iteration number averaged per face of the mesh on the left of Figure 18, and the landmark error plot on the left. The intensity registration is more complicated in this case. Nevertheless we can see that the algorithm still successfully reduces the intensity and landmark matching errors.

Example 6: (*Registration of partial human faces*) In this example, we test our registration method on another pair of inconsistent human faces, which are obtained from FIDENTIS 3D Face Database [1]. The first and second columns in Figure 19 show the moving human face and the target static human face respectively. The colormaps on each surfaces are given by their mean curvatures. We again perform conformal flattening [11] of the two surface meshes into 2D, as shown in the first row of Figure 20. The landmark correspondences in the 2D parameter domains are also shown. In this example, we have used $\alpha = 0.01, \beta = 0.1$, smoothing steps $M_1 = 1, M_2 = 5$; bounds $K_1 = 5, K_2 = 0.2$; free boundary subproblem for $N_1 = 5$ iterations; intensity subproblem for 5 iterations and overall iteration $N = 30$. The registration result is shown in the last column of Figure 19. It is the registered surface from the moving surface to the target static surface. The colormap on the surface is given by the curvature mismatching error. The mismatching error is small, indicating the curvatures are accurately matched. The registration result in the 2D domain is shown in the second row of Figure 20. The blue mesh is

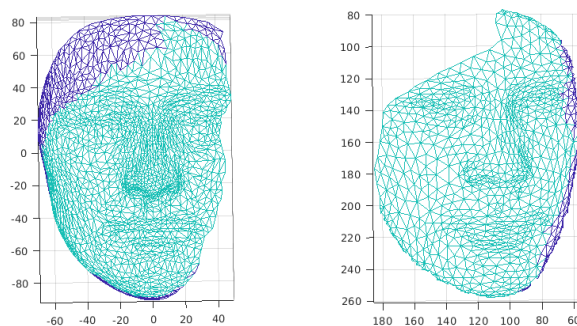


Fig. 17 Corresponding regions on the moving and static human faces in Example 5. The green region on left shows the corresponding region on the moving surface. The green region on the right shows the corresponding region on the target surface.

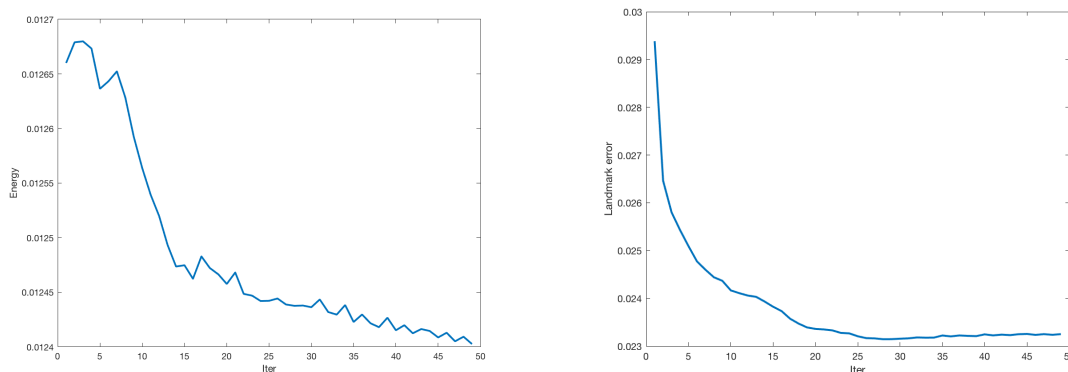


Fig. 18 Energy and landmark error plots for the human face experiment in Example 5 against iteration number. Energy is averaged per face. The left shows the overall energy versus iterations. The right shows the landmark mismatching error versus iterations.

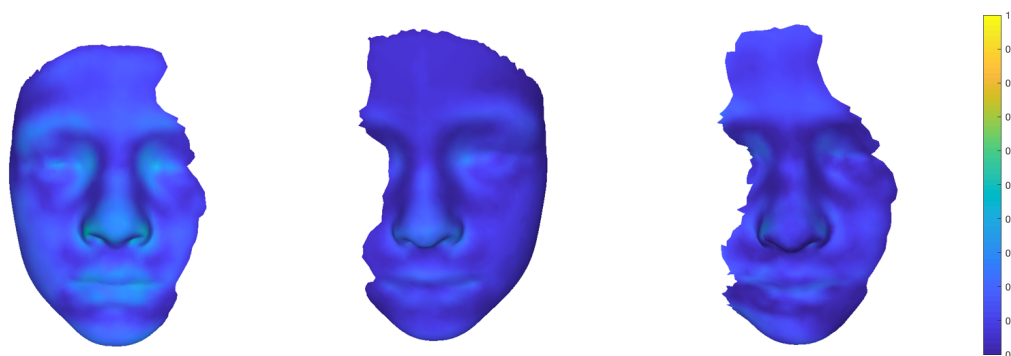


Fig. 19 Surface registration for another pair of inconsistent human faces in Example 6. The left shows the input moving surface. The middle shows the target static surface. The right shows the difference of intensities on the registered surface.

transformed mesh from the moving mesh under the registration map. The red mesh is the 2D mesh of the target surface under the conformal parameterization. The intersection region of the two meshes is the region of correspondence amongst the two human faces. We also display the energy plot against iteration number averaged per face of the mesh on the left of Figure 22, and the landmark error plot on the left. The intensity registration is more complicated in this case. Nevertheless we can see that the algorithm still successfully reduces the intensity and landmark matching errors.

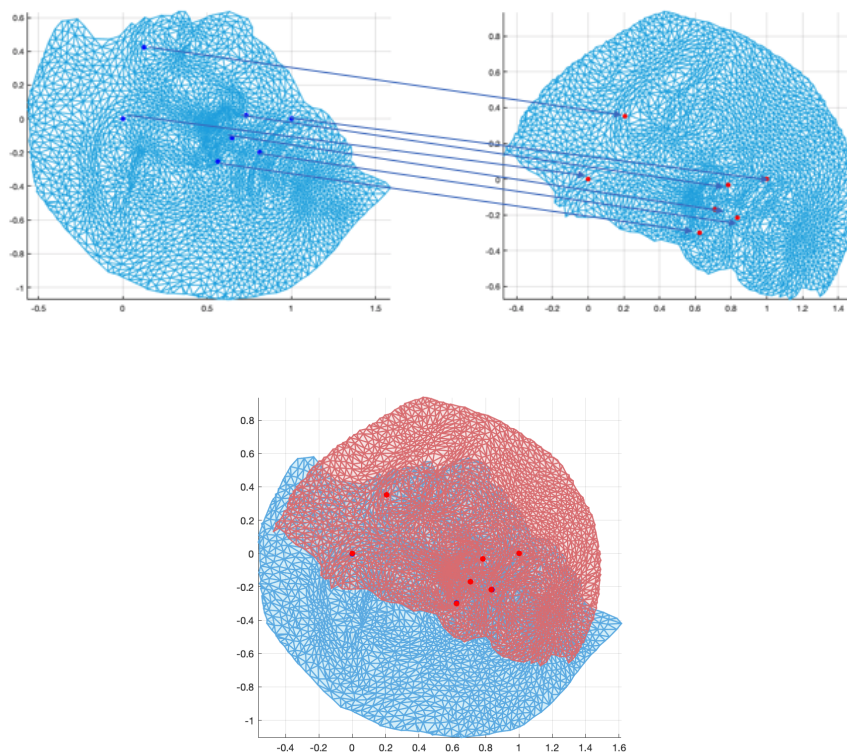


Fig. 20 The first row shows the conformal parametrizations of the moving and static human faces in Example 6 respectively. The landmark correspondences in the 2D parameter domains are also displayed. The registration result in the 2D domain is shown in the second row. The blue mesh is transformed mesh from the moving mesh under the registration map. The red mesh is the 2D mesh of the target surface under the conformal parametrization.

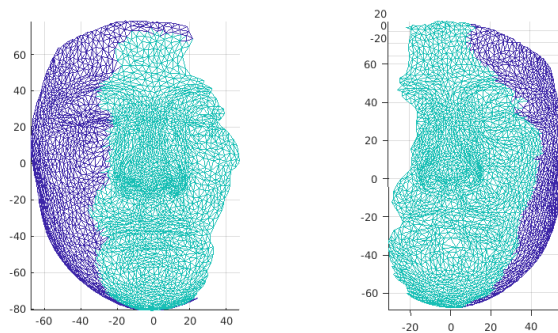


Fig. 21 Corresponding regions on the moving and static human faces in Example 6. The green region on left shows the corresponding region on the moving surface. The green region on the right shows the corresponding region on the target surface.

7 Conclusion

We have proposed a deformation model that is able to control both angle and area distortion and allow free boundary movement, which is further developed into a registration algorithm used for domains that are not in any natural global bijective correspondence. The key is to use Beltrami coefficient for smoothness and the mapping differential singular values for free boundary. Experimental results have been given to show the effectiveness of our approach.

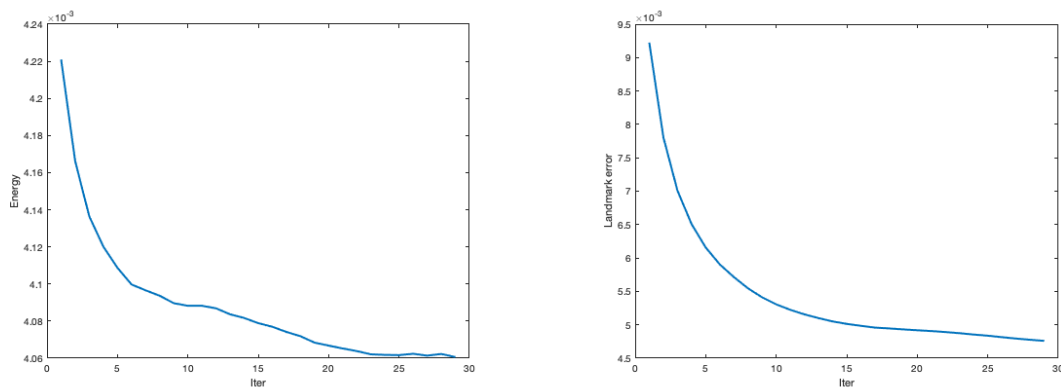


Fig. 22 Energy and landmark error plots for the human face experiment in Example 6 against iteration number. Energy is averaged per face. Energy is averaged per face. The left shows the overall energy versus iterations. The right shows the landmark mismatching error versus iterations.

References

1. Fidentis database. https://www.facebase.org/facial_norms/notes/6262. Accessed: 2018-10-01
2. Amberg, B., Romdhani, S., Vetter, T.: Optimal step nonrigid icp algorithms for surface registration. In: 2007 IEEE Conference on Computer Vision and Pattern Recognition, pp. 1–8. IEEE (2007)
3. Astala, K., Iwaniec, T., Martin, G.: Elliptic Partial Differential Equations and Quasiconformal Mappings in the Plane (PMS-48). Princeton University Press (2008)
4. Bronstein, A.M., Bronstein, M.M., Kimmel, R.: Generalized multidimensional scaling: a framework for isometry-invariant partial surface matching. *Proceedings of the National Academy of Sciences* **103**(5), 1168–1172 (2006)
5. Choi, P.T., Lam, K.C., Lui, L.M.: Flash: Fast landmark aligned spherical harmonic parameterization for genus-0 closed brain surfaces. *SIAM Journal on Imaging Sciences* **8**(1), 67–94 (2015)
6. Desbrun, M., Meyer, M., Alliez, P.: Intrinsic parameterizations of surface meshes. In: *Computer graphics forum*, vol. 21, pp. 209–218. Wiley Online Library (2002)
7. Gu, X., Yau, S.T.: Global conformal surface parameterization. In: *Proceedings of the 2003 Eurographics/ACM SIGGRAPH symposium on Geometry processing*, pp. 127–137. Eurographics Association (2003)
8. Igarashi, T., Moscovich, T., Hughes, J.F.: As-rigid-as-possible shape manipulation. In: *ACM transactions on Graphics (TOG)*, vol. 24, pp. 1134–1141. ACM (2005)
9. Kovalsky, S.Z., Aigerman, N., Basri, R., Lipman, Y.: Large-scale bounded distortion mappings. *ACM Transactions on Graphics (TOG)* **34**(6), 191 (2015)
10. Lam, K.C., Lui, L.M.: Landmark-and intensity-based registration with large deformations via quasi-conformal maps. *SIAM Journal on Imaging Sciences* **7**(4), 2364–2392 (2014)
11. Lévy, B., Petitjean, S., Ray, N., Maillot, J.: Least squares conformal maps for automatic texture atlas generation. In: *ACM transactions on graphics (TOG)*, vol. 21, pp. 362–371. ACM (2002)
12. Li, H., Sumner, R.W., Pauly, M.: Global correspondence optimization for non-rigid registration of depth scans. In: *Computer graphics forum*, vol. 27, pp. 1421–1430. Wiley Online Library (2008)
13. Lipman, Y.: Bounded distortion mapping spaces for triangular meshes. *ACM Transactions on Graphics (TOG)* **31**(4), 108 (2012)
14. Lui, L.M., Lam, K.C., Wong, T.W., Gu, X.: Texture map and video compression using beltrami representation. *SIAM Journal on Imaging Sciences* **6**(4), 1880–1902 (2013)
15. Lui, L.M., Wen, C.: Geometric registration of high-genus surfaces. *SIAM Journal on Imaging Sciences* **7**(1), 337–365 (2014)
16. Ovsjanikov, M., Corman, E., Bronstein, M., Rodolà, E., Ben-Chen, M., Guibas, L., Chazal, F., Bronstein, A.: Computing and processing correspondences with functional maps. In: *SIGGRAPH ASIA 2016 Courses*, p. 9. ACM (2016)
17. Pennec, X., Cachier, P., Ayache, N.: Understanding the demons algorithm: 3d non-rigid registration by gradient descent. In: *International Conference on Medical Image Computing and Computer-Assisted Intervention*, pp. 597–605. Springer (1999)
18. Pinkall, U., Polthier, K.: Computing discrete minimal surfaces and their conjugates. *Experimental mathematics* **2**(1), 15–36 (1993)
19. Qiu, D., Lam, K.C., Lui, L.M.: Computing quasiconformal folds. *arXiv preprint arXiv:1804.03936* (2018)
20. Rabinovich, M., Poranne, R., Panozzo, D., Sorkine-Hornung, O.: Scalable locally injective mappings. *ACM Transactions on Graphics (TOG)* **36**(2), 16 (2017)
21. Rodolà, E., Cosmo, L., Bronstein, M.M., Torsello, A., Cremers, D.: Partial functional correspondence. In: *Computer Graphics Forum*, vol. 36, pp. 222–236. Wiley Online Library (2017)
22. Rusinkiewicz, S., Levoy, M.: Efficient variants of the icp algorithm. In: *3dim*, vol. 1, pp. 145–152 (2001)
23. Sorkine, O., Alexa, M.: As-rigid-as-possible surface modeling. In: *Symposium on Geometry processing*, vol. 4 (2007)
24. Thirion, J.P.: Image matching as a diffusion process: an analogy with maxwell’s demons. *Medical image analysis* **2**(3), 243–260 (1998)